Stability of Ice/Rock Mixtures with Application to a Partially Differentiated Titan

Joseph G. O'Rourke, David J. Stevenson

Division of Geological and Planetary Sciences, California Institute of Technology, Pasadena, CA 91125, USA

Abstract

Titan's moment of inertia, calculated assuming hydrostatic equilibrium from gravity field data obtained during the Cassini-Huygens mission, implies an internal mass distribution that may be incompatible with complete differentiation. This suggests that Titan may have a mixed ice/rock core, possibly consistent with slow accretion in a gas-starved disk, which may initially spare Titan from widespread ice melting and subsequent differentiation. A partially differentiated Titan, however, must still efficiently remove radiogenic heat over geologic time. We argue that compositional heterogeneity in the major Saturnian satellites indicates that Titan formed from planetesimals with disparate densities. The resulting compositional anomalies would quickly redistribute to form a vertical density gradient that would oppose thermal convection. We use elements of the theory of double-diffusive convection to create a parameterized model for the thermal evolution of ice/rock mixtures with a stabilizing compositional gradient. Simulations are performed for a wide range of initial conditions to account for large uncertainties in material properties and accretionary processes. Ultimately, for realistic density gradients, double-diffusive convection in the ice/rock interior can delay, but not prevent, ice melting and differentiation, even if a substantial fraction of potassium is leached from the rock component. Consequently, Titan is not partially differentiated.

Keywords: Titan, interior, Saturn, satellites, Jupiter, satellites, Thermal histories

1. Introduction

Titan is Saturn's largest satellite, the second largest in our Solar System. The surface of Titan features stable liquid methane/ethane lakes, a hydrocarbon precipitation cycle comparable to Earth's hydrology, and myriad additional geologic features such as dune fields and mountainous terrain (Jaumann et al., 2009). From an astrobiology perspective, Titan is interesting as a modern analogue for pre-biotic Earth (Raulin et al., 2009). Titan has a thick nitrogen atmosphere, which must be sustained by the continuous production of methane (Atreya et al., 2006). Methane may be stored subsurface or perhaps more deeply in stable clathrate-hydrates along with other volatiles and episodically outgassed when internal heating causes melting (Gautier and Hersant, 2005; Tobie et al., 2006). Understanding Titan's fascinating surface, atmosphere, and chemistry requires knowledge of the evolution of its interior.

Measurements of the gravity field of Titan can place indirect constraints on the current structure of its interior. Titan's gravity harmonics were determined to degree 3 through careful tracking of the Cassini spacecraft during four flybys (Iess et al., 2010). The calculated ratio J_2/C_{22} is consistent with the value of 10/3 that is itself consistent with a gravity field dominated by a nearly hydrostatic quadrupole, although non-zero values of other degree 2 and 3 coefficients indicate that nonhydrostatic features are present. If hydrostatic equilibrium is assumed, however, then Titan's moment of inertia (MoI) factor is found to be C $\sim$ 0.34. Here, the MoI is $CM_sR_s^2$, where M_s and R_s respectively represent the mass and radius of Titan. Measurement of the tidal Love number k_2 from additional flybys reveals a relatively large response of the gravity field to the Saturnian tidal field, indicating the presence of a global, subsurface ocean (Iess et al., 2012). The decoupling of Titan's shell from its interior with an ocean may also explain Titan's long-wavelength topography (Nimmo and Bills, 2010), spin pole orientation (Bills and Nimmo, 2011), and Schumann resonance (Simoes et al., 2012).

The 2-σ error on J_2/C_{22} is about 3%, centered on 10/3 and dominated by the error in J_2, according to Iess et al. (2010). We can write $J_2 = J_{2,h}+J_{2,nh}$ and likewise $C_{22} = C_{22,h} + C_{22,nh}$, where "h" means hydrostatic and "nh" means non-hydrostatic, so $J_{2,h}/C_{22,h}$ is *exactly* 10/3. If the non-hydrostatic parts were completely uncorrelated, then the closeness of the observed value to 10/3 is highly significant and precludes a substantial error in MoI. If, on the other hand, the non-hydrostatic parts tend to be correlated (as they would be, for example, in the tidal heating model of Nimmo and Bills (2010) or if Titan has undergone True Polar Wander to the preferred orientation of the non-hydrostatic part of the MoI), then the small deviation away from 10/3 does not guarantee smallness of the non-hydrostatic part and the MoI is accordingly uncertain. Given the observed

power in degree 3 gravity, Iess et al. (2010) propose that the MoI could be as low as 0.33 and we adopt this as a plausible lower bound. The true MoI is likely to be smaller than 0.34, the value inferred from J_2/C_{22}, because this is a lower rotational energy state. Since a fully differentiated Titan may allow 0.33 (but perhaps not 0.34), the differentiation state of Titan is accordingly not yet determined from observation.

Titan's MoI can be compared to previous results regarding other icy satellites. In particular, Titan's MoI coefficient is intermediate to the previously-measured C ~ 0.31 for Ganymede (Anderson et al., 1996a) and C ~ 0.35 for Callisto (Anderson et al., 2001), where hydrostatic equilibrium was assumed *a priori* for the Galilean satellites. While Ganymede can easily be modeled as a differentiated satellite with an iron core under a rock shell and an outer ice layer (e.g., Sohl et al., 2002), models of a differentiated Callisto are not consistent with the reported MoI (e.g., Anderson et al., 2001). A proposed interior structure for Callisto features a rock/ice core with rock mass fraction near the close packing limit, with an overlying icy mantle that was depleted of rock by Stokes settling (Nagel et al., 2004). In this case, an ice/rock lithosphere in which density decreases with depth overlays the icy mantle. Titan might represent an intermediate case between differentiated Ganymede and undifferentiated Callisto. However, the inferred (and widely cited) partially differentiated state for Callisto is based on a gravity inversion that *assumes* $J_2/C_{22} = 10/3$, and perhaps the inferred MoI is incorrect. As for Titan, the sense of the error is likely to cause an overestimate of the MoI because non-hydrostatic contributions to J_2 and C_{22} are likely to be positive. At present, we cannot exclude the possibility that *all* large icy satellites are fully differentiated. (In this paper, we use that term to imply the complete separation of ice from rock; the further differentiation of an iron core from the rock is a separate issue that we do not address.) It should be noted that non-hydrostatic effects are more likely to be important in slowly rotating bodies (Titan and Callisto) relative to Ganymede because the hydrostatic effects scale as rotational frequency squared for both tides and synchronous rotation (Gao and Stevenson, 2012, and in preparation).

Certainly Callisto and Ganymede are different in appearance and Callisto, like Titan, lacks a global magnetic field. Relative differences in the experienced intensity of the Late Heavy Bombardment (LHB) may explain the Ganymede/Callisto dichotomy. In the so-called "Nice model," the gas giant planets swiftly realigned once Jupiter and Saturn crossed their mean motion resonance $\sim$700 million years after planetary formation, quickly causing the outward migration of Uranus and Neptune and the evolution of Jupiter and Saturn's orbital eccentricities (Tsiganis et al., 2005). The ensuing destabilization of the planetesimal disk and the asteroid belt caused the LHB of both the outer and inner solar system (Gomes et al., 2005). Ganymede is closer to Jupiter than Callisto, so it likely suffered considerably more high-energy impacts during the LHB. For assumptions about the planetesimal disk consistent with the Nice model, the differences in received energy during the LHB are sufficient to cause Ganymede to differentiate, while Callisto's rock and ice components may remain unmixed (Barr and Canup, 2010). If Titan survived both accretion and the LHB without melting the ice in its deep interior, then it could have remained partially differentiated like Callisto, at least initially.

Gas giant satellites like Titan were accreted from the outskirts of the disk of material surrounding their parent planets. Nascent gas giant planets must accrete enough rock such that they can also accumulate large amounts of gas, principally hydrogen and helium, before the dissipation of the protoplanetary disk, which had a lifetime of a few million years (e.g., Lissauer and Stevenson, 2007; Lunine et al., 2009). In the core-nucleated gas accretion model, for instance, the formation of Saturn began with the accretion of kilometer-sized rocky planetesimals from the minimum mass sub nebula (MMSN) (e.g., Lissauer and Stevenson, 2007). However, if gas giant satellites were accreted from the outskirts of a disk of planet-forming material as dense and gas-rich as the MMSN, then Jupiter's Galilean satellites (and, by analogy, Titan) would have formed quickly and hot (e.g., Mosqueira and Estrada, 2003a) and therefore differentiated.

Internal structure models for Titan often assume widespread ice melting and thus differentiation. Many studies investigated the thermal evolution of Titan assuming a large silicate/iron core (e.g., Sohl et al., 2003; Tobie et al., 2005), before MoI data from Iess et al. (2010) cast doubt on such models. Convection in a silicate core has been invoked to melt clathrate hydrates and cause episodic outgassing of methane (Tobie et al., 2006). Another class of models assumes that Titan contains a large core of hydrated silicates, chiefly the serpentine mineral antigorite (Grindrod et al., 2008; Fortes et al., 2007; Castillo-Rogez and Lunine, 2010; Fortes, 2012; Tobie et al., 2012). Serpentinization of silicates in icy satellites is likely to be rapid in the presence of liquid water, e.g. during differentiation or subsequent hydrothermal convection (Ransford et al., 1981; Travis and Schubert, 2005), because the serpentinization reaction promotes crack formation and increasing material permeability (MacDonald and Fyfe, 1985). An interior dominated by hydrated silicates is consistent with constraints on Titan's chemical evolution (e.g., Fortes et al., 2007; Fortes, 2012). But a partially differentiated Titan, in which Titan's deep interior is a mixture of ice and rock, is still consistent with the gravity data (Iess et al., 2010), and such models have not been fully vetted.

The accretion of undifferentiated icy satellites is often assumed to have occurred in a "gas-starved" disk, where material similar to that found in the gas giant's feeding zone is fed to the accretion process over millions of years. The resulting long satellite accretion timescales allow many of the Galilean satellites, particularly Cal-

listo, to avoid complete differentiation (e.g., Canup and Ward, 2002). In another model, the major satellites of Jupiter and Saturn formed in a solid-enhanced minimum mass planetary nebula, avoiding differentiation as satellites open gaps in the nebula (Mosqueira and Estrada, 2003a,b). With a particular compositional gradient in the initial circumplanetary disc, the compositions of the major Saturnian satellites can be roughly reproduced (Mosqueira et al., 2010). In any model, accretion must also be delayed to escape intense, but short-lived, radiogenic heating from the decay of ^{26}Al if an icy satellite is to avoid complete differentiation (e.g., McKinnon, 1997; Barr and Canup, 2008). Despite myriad threats to unmelted ice, slow accretion in a gas-starved disk permits the formation of a partially differentiated Titan (Barr et al., 2010).

The purpose of this study is to determine whether a partially differentiated Titan is stable over geologic time. After accretion, the internal ice/rock mixture must efficiently expel radiogenic heat, which would otherwise melt the ice and allow irreversible sinking and separation of the rock component. Because the major Saturnian satellites are remarkably heterogenous, we argue that Titan likely accreted from planetesimals with disparate rock mass fractions. Even without that heterogeneity, there may be a tendency to form a stably stratified interior at the outset. Soon after accretion, a stabilizing density gradient would be established in which rock mass fraction increases with depth. Aspects of the theory of double-diffusive convection allow us to formulate a one-dimensional, parameterized thermal evolution model in which a convecting layer slowly grows to encompass the entire ice/rock interior. We perform simulations for a large set of initial conditions because of uncertainties in key parameters and to analyze the sensitivity of our results. Finally, we discuss alternatives to a partially differentiated Titan and consider possible implications for other icy satellites.

2. Theoretical formulation

Our simple model assumes that Titan is a sphere of radius R_s and mass M_s, consisting of an undifferentiated ice/rock interior with radius R_i and an overlying shell. The structure of the outer shell may be complicated, especially considering the likely presence of an ocean, but we do not need to model it in detail. We perform parametrized thermal evolution simulations to assess whether Titan can remain partially differentiated until the present. Stabilizing compositional gradients, caused by increasing rock mass fraction and thus density with depth, likely inhibit convection in Titan's ice/rock interior. Elements from the theory of double-diffusive convection are incorporated to model thermal evolution with this complication. Although this simple model will not precisely reconstruct the thermal history of Titan, it does provide a first-order test of the hypothesis of partial differentiation.

2.1. Establishment of vertical density gradients

The major Saturnian satellites exhibit significant compositional heterogeneity. The mass-weighted density of the major Saturnian satellites, excluding Titan (Mimas, Enceladus, Tethys, Dione, Rhea, Hyperion, Iapetus, and Phoebe), is $\rho_{av} \approx 1{,}270$ kg m^{-3} (Jacobson, 2004). The average densities of each satellite vary widely, from less than 1,000 kg m^{-3} to over 1,300 kg m^{-3}. In fact, the inner satellites (the first five of the aforementioned) and Saturn's almost-pure water ice rings may have been formed from tidal stripping of a Titan-sized satellite that was lost within Saturn's classical Roche limit (Canup, 2010). Titan's mean density is ∼1,881 kg m^{-3}, but its uncompressed density is not much higher than the densities of the other Saturnian satellites.

Since Titan was plausibly formed from planetesimals of size and composition similar to these satellites, lateral density anomalies as large as 10% likely existed after accretion. These unstable anomalies drive a flow that will restructure the ice/rock mixtures so that more dense mixtures underlie less dense mixtures, in a length of time that scales as

$$t_f \sim \frac{\mu}{\Delta\rho_{lat} g D}, \tag{1}$$

where μ is viscosity, $\Delta\rho_{lat}$ is the horizontal density anomaly, g is gravitational acceleration, and D is the length scale of the anomalies. A competing process is the Stokes settling of the dense rock fragments from the ice/rock mixture. Using the usual Stokes settling velocity, the time in which the rock fragments settle out of the mixture may be written as

$$t_s \sim \frac{\mu D}{\Delta\rho g R^2}, \tag{2}$$

where $\Delta\rho$ is the density difference between the ice and the rock (on the order of 1,000 to 2,000 kg m^{-3}) and R is the radius of the rock fragments. For R ∼ 1 m and D ∼ 100 km, the formation of the vertical density gradients overwhelms the Stokes settling of the rocks if the lateral density anomaly is greater than only one part in ten billion of the density difference between the ice and rock, i.e. $t_f < t_s$ if $\Delta\rho_{lat} > 10^{-10}\Delta\rho$. Clearly, this is easily achieved.

Mixing during accretion will not homogenize the differences arising from large planetesimals. Importantly, *lateral* differences during the accretion lead to *vertical* differences in ice/rock ratio after settling, even if individual impact events mix vertically. Therefore, models of Titan's thermal evolution must consider the existence of up to ∼10% stabilizing density gradients in Titan's ice/rock interior initially (and even smaller effects are still very important because thermal expansion of ice produces much smaller density differences). A vertical density gradient, where density increases with depth, opposes thermal buoyancy, inhibiting convection and thus preventing substantial heat transfer. If radiogenic heat is not removed from the system, then the ice in

Titan's deep interior will melt, especially if low melting point components such as ammonia are present. The liberated rock components will sink as the melt percolates upwards. Runaway differentiation can occur if the gravitational energy released by the sinking of the rock component is sufficient to melt more ice (Friedson and Stevenson, 1983), but complete differentiation may occur without invoking runaway differentiation if convection is sufficiently suppressed.

2.2. Double-diffusive convection applied to Titan

The theory of double-diffusive convection was originally developed to elucidate various phenomena in oceanography (Stern, 1960). In general, double-diffusive phenomena occur in the presence of two opposing density gradients, where the two responsible components have different molecular diffusivities (e.g., Turner, 1974). The theory has been extended to the dynamics of magma chambers and stellar interiors (e.g., Spiegel, 1972; Schmitt, 1983; Turner, 1985), but it remains most often utilized in oceanography. For instance, in Earth's high latitudes, the polar oceans are composed of cold, fresh water overlying warm, salty water (e.g., Schmitt, 1994). In the presence of the stabilizing salinity gradient, convective motions resembling Rayleigh-Bénard convection arise after a stage of steady oscillating motions in layers cooled from above (Veronis, 1968; Noguchi and Niino, 2010). These well-mixed, convecting layers increase in thickness and frequently merge with neighboring layers of equal density. This is known as the "diffusive-layer" mode, in which salinity, the stabilizing component, has a much lower molecular diffusivity than temperature, the component driving convection.

Titan's deep interior features analogous opposing temperature and compositional gradients. The compositional gradient is simply a measure of the increasing rock mass fraction in the ice/rock mixture with depth. Although a temperature gradient can induce particle motion through interfacial premelting (Rempel et al., 2001), the relevant time scales are far too long for application to icy satellites. Hence, the molecular diffusivity associated with the rock component is effectively zero. Because the molecular diffusivity of salt is nonzero, in contrast, complicated temperature and salinity profiles exist in the ocean (e.g., Huppert and Turner, 1981), with time-dependent fluxes of salt and temperature across diffusive interfaces between the multiple convecting layers (e.g., Worster, 2004). Regardless, the term "double-diffusive" is still applicable to our model of convection in the presence of a stabilizing gradient. As outlined below, aspects of the theory applied to Titan do not depend on the molecular diffusivity of the component opposing temperature.

In Titan, double-diffusive convection occurs in the presence of a stabilizing rock mass fraction gradient as its deep interior is cooled from above or heated from within. The density within the ice/rock interior is a linear function of rock mass fraction and temperature (Turner, 1974):

$$\rho = \rho_0(1 - \alpha\Delta T + \beta\Delta S), \tag{3}$$

where ρ_0 is the density at some reference depth, α is the coefficient of thermal expansion, and $\beta = (1/\rho)(\partial\rho/\partial S)$ is the coefficient of compositional expansion, analogous to α, associated with the change in rock mass fraction. The change of density due to pressure alone can be omitted because it does not contribute to the convective stability and is in any event too small to greatly affect the form of the convective motions. Table 1 contains numerical values of these coefficients and other constants used in this study. The rock mass fraction may be calculated (Barr et al., 2010):

$$S = \frac{\rho_r(\bar{\rho} - \rho_i)}{\bar{\rho}(\rho_r - \rho_i)}, \tag{4}$$

where $\bar{\rho}$ is the average density, ρ_r is the rock density, and ρ_i is the ice density. High-pressure ice phases V, VI, and VII exist within Titan's deep interior; a representative density ρ_i = 1,400 kg m^{-3} is chosen in accord with Barr et al. (2010). Although the mineralogy of Titan's rock component is not completely known, CI carbonaceous chondrites and Prinn-Fegley rock, an assemblage that models condensate from the proto-Jovian nebula, are possible analogues, motivating the choice ρ_r = 3,300 kg m^{-3} (Mueller and McKinnon, 1988; Barr et al., 2010).

A quick calculation with Eqs. 3 and 4 reveals why compositional gradients make melting much more likely in a partially differentiated Titan. A ~10% density contrast across Titan's interior corresponds to $\Delta S \sim 10^{-1}$ between ice/rock parcels at the top and bottom of the mixture. So, an (impossible) temperature increase of $\Delta T \sim 10^3$ K is required before compositionally dense parcels can become buoyant.

For cooling from above or for steady heating from within, but with the top temperature kept constant, convection begins at the top of Titan's ice/rock interior. With a linear density distribution, an equation for a measure of the initial stability gradient may be written (Turner, 1973):

$$N_S^2 = -g\beta\frac{dS}{dz}, \tag{5}$$

where N_S is a frequency of oscillation. When heat flows out of the top of the convecting layer, the associated buoyancy flux may be calculated (Turner, 1973):

$$B = -\frac{g\alpha H}{\rho C_p}. \tag{6}$$

As cooling continues from above, a well-mixed convecting layer grows with height (Turner, 1973):

$$h = \left(\frac{2Bt}{N_S^2}\right)^{1/2}. \tag{7}$$

Therefore, the rate of the growth of the convecting layer may be calculated:

$$\frac{dh}{dt} = \left[\frac{\alpha H}{2\rho C_p \beta (dS/dz) t}\right]^{1/2}. \tag{8}$$

Constant	Definition	Value	Units	Ref.
A	Activation parameter for ice	25	-	[1]
κ	Thermal diffusivity	10^{-6}	$m^2\ s^{-1}$	[1]
α	Coefficient of thermal expansivity	10^{-4}	K^{-1}	[1]
β	Coefficient of compositional expansivity	1.1	-	*
M_s	Mass of Titan	1.345×10^{23}	kg	[2]
R_s	Radius of Titan	2575	km	[2]
R_i	Radius of ice/rock interior	2000	km	*
ρ_i	Density of ice	1400	kg m^{-3}	[2]
ρ_r	Density of rock	3300	kg m^{-3}	[2]
$C_{p,i}$	Specific heat of ice	2100	J $kg^{-1}\ K^{-1}$	[2]
$C_{p,r}$	Specific heat of rock	900	J $kg^{-1}\ K^{-1}$	[3]

Table 1: List of key model constants. References: 1. Friedson and Stevenson (1983), 2. Barr et al. (2010), 3. Grindrod et al. (2008), *this study.

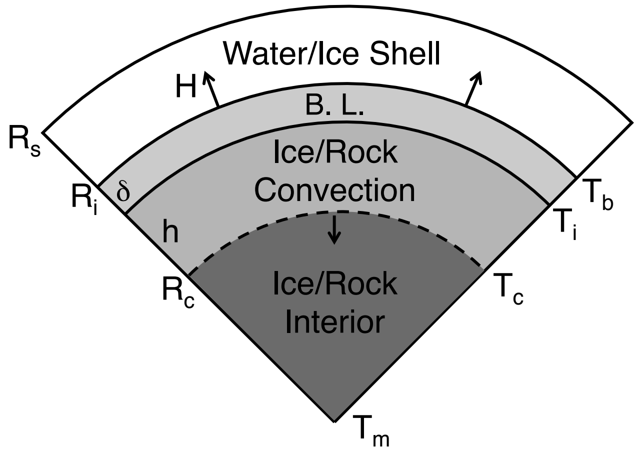

Figure 1: Cartoon showing the assumed structure of Titan after the initialization of double-diffusive convection in the interior ice/rock region, before the convecting layer has grown to encompass the entire interior. Dimensions are not to scale and the overlying water/ice shell is not drawn in detail. Key model parameters are indicated as used in the text.

Figure 1 shows the internal structure of Titan after double-diffusive convection has proceeded for some time. The radius of the ice/rock interior is R_i. The non-convecting ice/rock core has radius R_c, where T_c and T_m respectively represent the outer and inner temperatures. A thermal boundary layer exists between the convecting outer shell and the convecting ice/rock interior with thickness δ. The temperature at the top of the thermal boundary layer, T_b, is held constant, while the temperature of the convecting layer is T_i. Parametrized thermal evolution models typically assume adiabatic temperature gradients in convecting layers, but these temperature increases with depth are negligible.

2.3. Governing equations

The governing equation is the conservation of energy equation for the convecting ice/rock layer:

$$4\pi R_i^2 H = \frac{4\pi}{3}\bar{\rho}(R_i^3 - R_c^3)\left(Q - C_p\frac{dT_l}{dt}\right) - \rho_i f_i L_m, \quad (9)$$

where H is the heat flux out of the convecting ice/rock layer into the overlying shell, Q is radiogenic heat production, f_i is the volume of melted ice, and L_m is the latent heat of melting. The specific heat of the ice/rock mixture is a mass-weighted average (Barr and Canup, 2008):

$$C_p = SC_{p,r} + (1-S)C_{p,i}, \quad (10)$$

where $C_{p,r}$ and $C_{p,i}$ are the specific heats of the rock and ice components, respectively. Assuming that no melting occurs, we can conveniently rewrite Eq. 9:

$$C_p\frac{dT_l}{dt} = Q - \frac{3H}{\bar{\rho}}\frac{R_i^2}{R_i^3 - R_c^3}. \quad (11)$$

We consider contributions to radiogenic heat production from ^{40}K, ^{235}U, ^{238}U, and ^{232}Th. Radiogenic heating in the ice/rock mixture may be calculated (e.g., Barr and Canup, 2008):

$$Q(t) = S\sum_n c_{n,0}P_{n,0}\exp(-\lambda_n t), \quad (12)$$

where, for the nth isotope, $c_{n,0}$ is the initial abundance, $P_{n,0}$ is the initial specific heat production, and λ_n is the decay constant. Table 2 lists the constants used to calculate radiogenic heat production. Because contact between silicates and ammonia/water liquid can leach volatile ^{40}K out of the rock component (e.g., Engel et al., 1994), we multiply the initial abundance of potassium by f, a depletion factor. Figure 2 shows representative temperature increases over 4.5 Gyr for $S=1.0$ and 0.8 from radiogenic heat production with $f=1.0$, 0.7, and 0.3.

2.4. Thermal evolution of Titan's ice/rock interior

The thermal evolution the ice/rock mixture within Titan may be simulated with a one-dimensional parametrized model. A critical parameter, subject to large uncertainty, is the viscosity of the ice/rock mixture. Although the deformation of ice is non-Newtonian under the conditions of Titan's deep interior, it can be

Isotope	$c_{n,0}$ [ppb]	$P_{n,0}$ [μW/kg]	λ_n [1/Gyr]
^{238}U	16.91	93.7	0.155
^{235}U	5.275	569	0.985
^{232}Th	38.71	26.9	0.0495
^{40}K $\rightarrow$ ^{40}Ar	813.8	1.02	0.0581
^{40}K $\rightarrow$ ^{40}Ca	813.8	26.69	0.4962

Table 2: Constants used to calculate radiogenic heat production, adapted from Barr and Canup (2008).

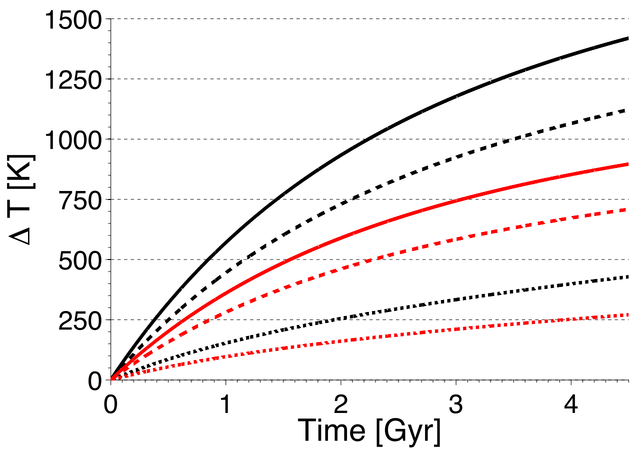

Figure 2: Temperature increase in a parcel of rock (black, $S = 1.0$) and in an ice/rock mixture with $S = 0.8$ (red). Solid, dashed, and dotted lines respectively represent $f = 1.0$, 0.7, and 0.3.

modeled with an Arrhenius-like equation for low strain rates (Friedson and Stevenson, 1983):

$$\eta = \frac{\nu_0}{\rho} \exp\left[A\left(\frac{T_m}{T} - 1\right)\right], \tag{13}$$

where A is an activation parameter and T_m is the melting point of water ice, calculated using data from Petrenko and Whitworth (1999). For conditions appropriate to icy satellites, adding rock particles to a water ice matrix may cause viscosity to increase by an order of magnitude (Friedson and Stevenson, 1983), but we do not explicitly model these effects in this study.

At first, a conductive boundary layer grows with thickness $\delta \sim \sqrt{\kappa t}$ at the top of the ice/rock interior. The conductive heat flux out of the boundary layer is

$$H = \frac{k\Delta T}{\delta}, \tag{14}$$

where $k = \kappa\rho C_p$ is thermal conductivity and κ is thermal diffusivity. The initial growth of the conductive boundary layer stops and convection begins when the Rayleigh number for the boundary layer reaches a critical value, i.e.,

$$Ra_c = \frac{g\alpha\Delta T\delta_c^3}{\eta(T)\kappa} = 10^3, \tag{15}$$

where ΔT is the temperature contrast across the boundary layer and δ_c is the critical thickness of the boundary layer.

After convection begins, the viscosity contrast between the convecting ice/rock mixture and the overlying shell of high pressure ice is less than the ~4 orders of magnitude required to produce a stagnant lid. So, the heat flux is given by the following equation (Friedson and Stevenson, 1983):

$$H = 0.1k(\Delta T)^{4/3}\left(\frac{g\alpha}{\eta(T_l)\kappa}\right)^{1/3}, \tag{16}$$

where $\Delta T = T_b - T_i$ is the temperature contrast driving convection. The thickness of the thermal boundary layer, δ, can be calculated using the condition for convective instability

$$\frac{g\alpha\Delta T\delta_l^3}{\eta(T_l - 0.5\Delta T)\kappa} = 10^3. \tag{17}$$

In reality, the thermal evolution of the ice shell above this thermal boundary layer is complicated. Titan likely has an shell consisting of an outer ice I layer, an ocean, and a mantle of high-pressure ice polymorphs (e.g., Iess et al., 2012). Convection in the ice I shell is expected for small grain sizes (Barr and McKinnon, 2007; Mitri and Showman, 2008), but the long-wavelength topography of Titan implies shell thickness variations that convection might eliminate, indicating that Titan's ice I shell may be currently conductive (Nimmo and Bills, 2010). Possibly this shell is at least in part clathrate hydrate, which has different transport properties. If the mantle of high-pressure ice is convecting, then a system of equations, for the convective instability of and temperature contrasts across the thermal boundary layers at the interface with the ice/rock interior, is necessary to precisely calculate the thermal evolution of Titan. Because our focus is on the thermal evolution of Titan's deep interior, we assume for simplicity that T_b is constant in all simulations.

3. Numerical models

Simulations are performed to calculate the thermal history of Titan's ice/rock interior for 4.5 Gyr. The model described above was numerically iterated with a time step of 1 Myr. Internal temperatures are compared to the phase diagram for pure water ice from Petrenko and Whitworth (1999) at each time step to determine whether melting occurs. Titan, as a whole, has $\bar{\rho} = 1{,}881$ kg m^{-3} and $S \approx 0.44$. We assume that Titan is

initially composed of an outer shell with a thickness of 575 km and a density of 1,200 kg m^{-3}. Therefore, R_i = 2,000 km and $S \approx 0.82$ in the ice/rock interior. The average density of the ice/rock interior, $\bar{\rho}$ = 2,653 kg m^{-3}. In this simple two-layer model, the normalized moment of inertia coefficient $C \approx 0.343$. The melting temperatures of water ice are ∼280 and 500 K at pressures of ∼0.7 and 4.7 GPa, respectively, which are the conditions at the top and bottom of the ice/rock interior.

A wide parameter space was explored by varying the initial conditions for hundreds of simulations. The temperature at the top of the thermal boundary layer in the ice/rock interior was fixed at T_b = 200 K, but the effects of different initial temperature gradients were explored by using both $T_m(0)$ = 200 and 125 K, as suggested by models of Titan's accretion (Mitri et al., 2010). Initial rock mass fraction gradients were imposed that produced effective density changes throughout the ice/rock interior as large as $\Delta\rho_s \sim 0.1\bar{\rho}$ (i.e., ∼10%). An initial temperature gradient, if present, also produces an effective density change of $\Delta\rho_t \sim \alpha\Delta T_i$, where $\Delta T_i = T_b - T_m(0)$. In some simulations, no initial compositional gradient was imposed. Because of the large uncertainty on the viscosity of ice/rock mixtures, we tested effective viscosities near melting in the range $\nu_0 = 10^{11}$ to 10^{15} Pa s. (Even larger values increase the likelihood of melting and lower values are much lower than physically plausible.) To account for the possibility of potassium leaching and uncertainties in the rock mineralogy, we conducted simulations using three different depletion factors: f = 1.0, 0.7, and 0.3. Guided by the results of these simulations, we construct some plausible present-day internal structure models for Titan.

4. Results

The following sections summarize the results of our simulations, beginning with the presentation of four representative thermal histories. Then, we discuss the effects of various initial conditions using a large number of simulation results. Finally, simulations in which melting occurred are analyzed to determine the details of melting in the ice/rock interior.

4.1. Sample thermal histories

Four examples of calculated thermal histories are shown in Fig. 3. In each simulation, a convecting layer with constant temperature grows over time, eventually encompassing the entire ice/rock interior. From 2.5 to 4.5 Gyr, this convecting ice/rock layer cools monotonically. Underneath the convecting layer, temperatures increase from radiogenic heating, although the initial linear temperature gradient is preserved. No melting occurs in any of these four examples within 4.5 Gyr because the convecting layer grows fast enough to encompass the entire interior before temperatures in the non-convecting layer increase sufficiently to cause widespread melting and differentiation.

Comparisons between pairs of these simulations illuminate the effects of varying the magnitude of compositional gradients, potassium depletion, and initial temperature gradients. Simulations shown in panels A and B, for instance, both have f = 1.0, $\nu_0 = 10^{14}$ Pa s, and $T_m(0)$ = 125 K. Panel A features a ∼1% compositional gradient, i.e., $\Delta\rho_s = 0.01\bar{\rho}$, whereas the initial density gradient in panel B is only the result of the initial temperature gradient. The growth of the convecting layer is relatively delayed by ∼500 Myr in panel A, allowing an additional ∼100 K of heating in the ice/rock interior.

Panels A and C illustrate the effects of potassium depletion on the thermal evolution of an ice/rock interior with a ∼1% compositional gradient. All initial conditions are identical for both simulations, except f = 0.3 in panel C. The primary effect of potassium depletion is to slow the growth of the convecting layer because heating in the underlying, non-convecting layer is necessary to overcome the initial compositional gradient. Specifically, convection in the entire ice/rock interior is delayed by ∼1.25 Gyr. The maximum temperatures reached in the non-convecting ice/rock interior, however, are only slightly lower in panel C than in panel A. On the other hand, the temperature of the convecting layer is generally reduced in panel C, since the convecting layer is relatively thin; internal heating is lessened; and the incorporation of hot material from the non-convecting interior is more gradual.

Finally, panels C and D reveal the effects of varying the effective viscosity near melting. Both simulations include substantial potassium depletion (f = 0.3) and start with a ∼1% compositional gradient. While panel C features $\nu_0 = 10^{14}$ Pa s as usual, $\nu_0 = 10^{12}$ Pa s in panel D. With a lower viscosity, the convecting layer has a lower temperature and takes slightly longer to encompass the entire interior. In fact, convecting layer growth is faster for the first ∼500 Myr in panel D, but marginally slower thereafter. Thus, heat flux out of the convecting layer is relatively low after a period of relatively rapidly cooling and convecting layer growth. Compared to the other initial conditions, however, the sensitivity of the model to uncertainties in viscosity is very small.

4.2. Sensitivity to initial conditions

Figure 4 shows results from 810 simulations of the thermal evolution of Titan's ice/rock interior. The purpose of each panel is to illustrate whether or not melting occurs for a particular set of initial conditions. Horizontal axes indicate the range of density differences across the ice/rock interior induced by an initial compositional gradient, i.e., $\Delta\rho_s = 0$ to $0.03\bar{\rho}$. Each vertical axis represents a range of effective viscosities near melting, i.e., $\nu_0 = 10^{11}$ to 10^{15} Pa s. Blue squares signify simulations in which melting never occurred, whereas red squares represent simulations where widespread melting would have caused differentiation of Titan's ice/rock interior within 4.5 Gyr.

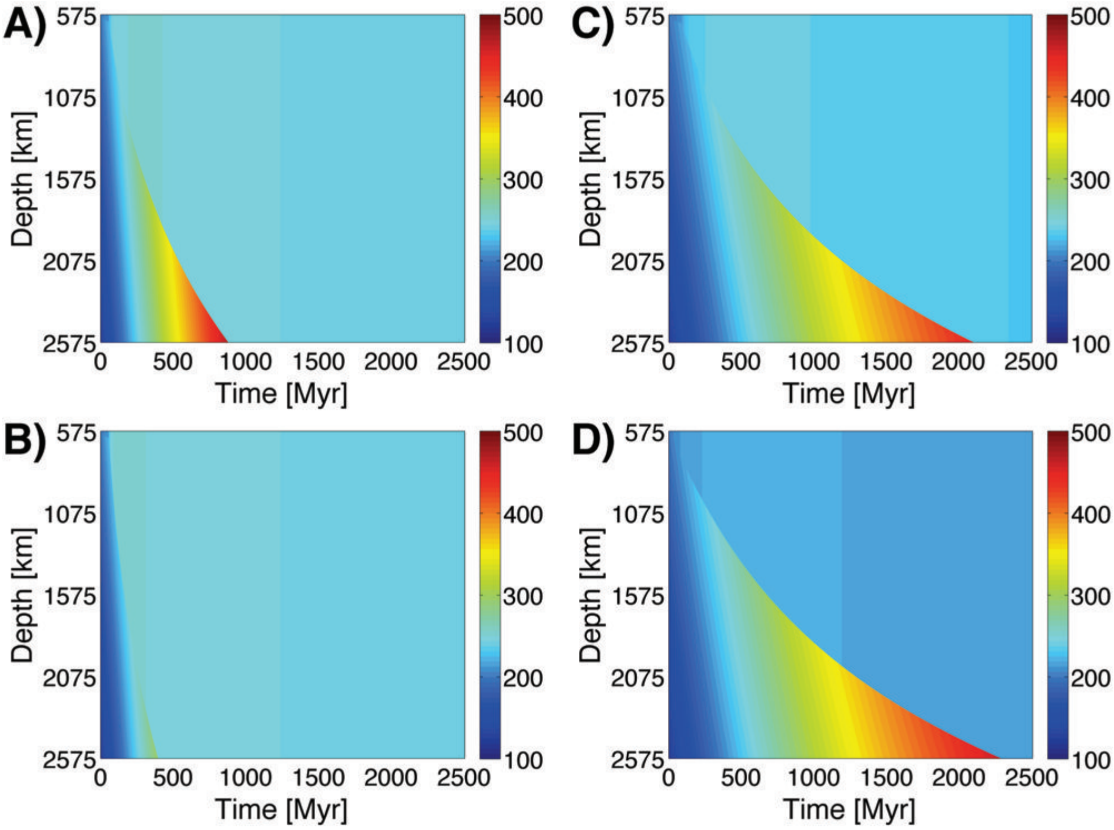

Figure 3: Representative results for simulations in which melting did not occur. Temperature profiles in Titan's ice/rock interior are plotted until the time after which the convecting interior simply cools monotonically. Default initial conditions for the four simulations are T_b = 200 K, $T_m(0)$ = 125 K, f = 1, $\log_{10}(\nu_0)$ = 14, and $\Delta\rho_s = 0.01\bar{\rho}$. Panel B has $\Delta\rho_s = 0$. Panel C has $f = 0.3$. Panel D has f = 0.3 and $\log_{10}(\nu_0)$ = 12.

Each panel represents a series of simulations that started with different initial temperature gradients and magnitudes of potassium depletion. The top and bottom rows of panels, for instance, have $T_m(0) = 125$ and 200 K, respectively. In general, melting is less likely to occur without an initial temperature gradient, because a temperature decrease with depth induces a density gradient that suppresses convection. High-viscosity simulations with low compositional gradients in panels D and E feature melting, while the corresponding simulations in panels A and B do not. The lack of a significant density gradient from compositional or temperature changes in these simulations causes the convecting layer to very quickly encompass the interior, homogenizing internal temperatures. Because the average internal temperature is comparatively high at first, however, melting occurs near the top of the ice/rock interior, where melting temperatures are relatively low.

Figure 4 also elucidates the effects of potassium depletion. From left to right, columns of panels have f = 1.0 (A and D), 0.7 (B and E), and 0.3 (C and F). Reducing the abundance of potassium in the rock component of the ice/rock interior only makes melting marginally less likely. As seen in the example thermal histories, potassium depletion only lengthens the time scales on which temperatures increase; the maximum temperatures reached in ice/rock interior are barely lessened. For any plausible choice of initial conditions, melting occurs if the initial compositional gradient is larger than $\sim$2%.

4.3. When and where melting occurs

Figure 5 contains more information about 173 simulations in which melting occurred for initial compositional gradients ranging from 1 to 10%. Specifically, panel A illustrates the time at which melting occurred and panel B shows the value of R_c, the radius of the non-convecting ice/rock interior, at the time when melting began. As in Fig. 4, six different sets of initial conditions were used. That is, black and red symbols respectively represent $T_m(0)$ = 125 and 200 K. For circular, square, and triangular markers, respectively, f = 1.0, 0.7, and 0.3. With large density gradients, the non-convecting ice/rock core always melts before the ice in the convecting layer.

The magnitudes of potassium depletion and the initial temperature gradient more strongly affect when melting occurs than where it begins. That is, increasing potassium depletion can delay melting by $\sim$500 Myr to 1.75 Gyr for a given initial compositional gradient, but the radius of the non-convecting core at the time when

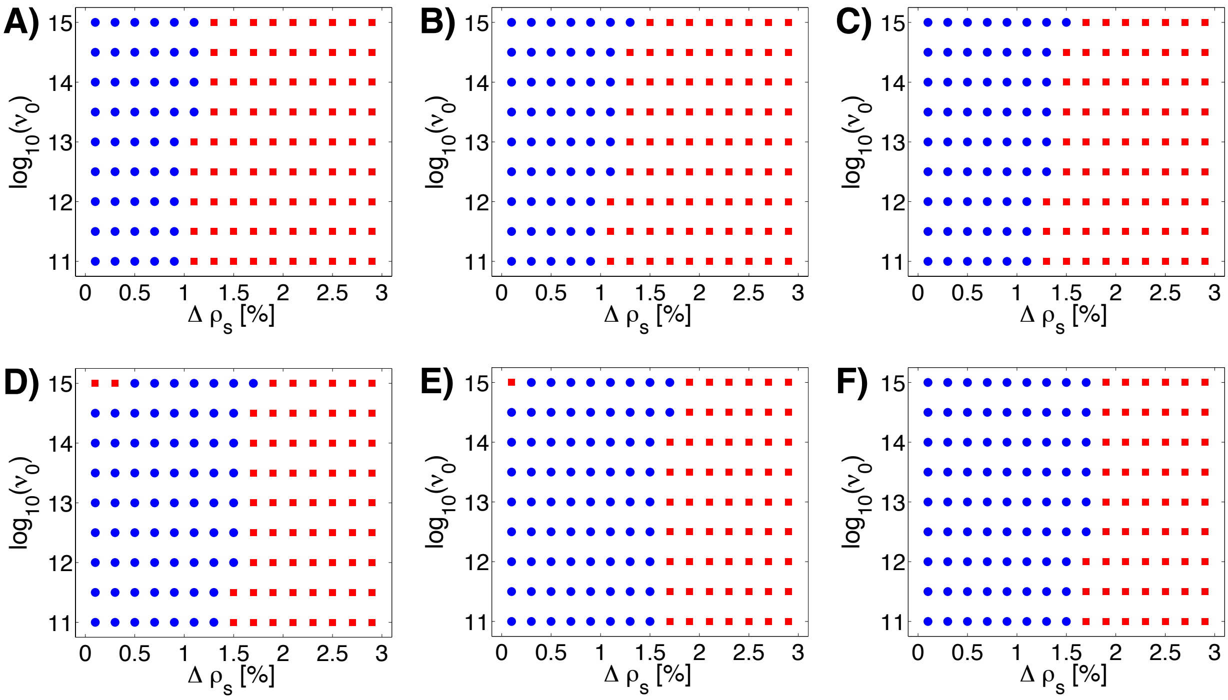

Figure 4: Sensitivity analyses results for 810 simulations exploring the effects of potassium depletion, effective viscosity near melting, and initial temperature and compositional gradients. In each panel, the horizontal axis shows the total density variation across the ice/rock interior produced by the initial compositional gradient and the vertical axis shows the dynamic viscosity near melting assumed for each simulation. Blue circles represent simulations in which no melting occurred in 4.5 Gyr; red squares signify simulations in which melting occurred at any point in the ice/rock interior. All simulations have T_b = 200 K. From left to right, each column of panels features f = 1.0, 0.7, and 0.3. The top and bottom rows of panels have $T_m(0)$ = 125 and 200 K, respectively. For initial compositional gradients producing $\Delta\rho_s > 0.02\bar{\rho}$, melting occurs during all simulations.

melting begins only slightly decreases. With no initial temperature gradient but a higher average internal temperature, melting occurs sooner, but the convecting layer has grown further before melting begins. As compositional gradients increase, melting occurs sooner, the convecting layer is thinner when melting occurs, and simulation sensitivity to the choice of initial conditions decreases.

5. Discussion

5.1. Stability of a partially differentiated Titan

A partially differentiated Titan is stable over geologic time if it can safeguard the ice in its deep interior from widespread melting caused by radiogenic heating. If thermal convection is vigorous throughout the entire ice/rock layer, then melting can be avoided. Even for small compositional gradients (∼1-1.5%) a convecting layer can grow to encompass the entire ice/rock interior before internal temperature profiles cross the melting curve of water ice. Larger compositional gradients (∼5-10%), however, are plausible since Titan likely accreted from heterogenous planetesimals. Thermal buoyancy simply cannot overcome these stabilizing gradients without causing ice melting and complete differentiation. The likely presence of ammonia in the ice component, which may significantly lower the melting temperature (e.g., Loveday et al., 2009), compounds the problem.

No plausible selection of initial conditions allows sufficiently efficient heat removal in the presence of a large compositional gradient. A substantial amount of heat-producing ^{40}K may be leached out of the rock component through contact with liquid water or ammonia-water solutions. Roughly 30% of the original abundance of potassium has been estimated to have been extracted from the silicates of Ganymede (Kirk and Stevenson, 1987) and Titan (Engel et al., 1994), and almost complete leaching of several elements has been suggested for Enceladus (Glein and Shock, 2010). A reduction in the magnitude of radiogenic heating may be important to preventing Titan's interior from reaching temperatures associated with silicate dehydration (Castillo-Rogez and Lunine, 2010), but, as seen in Fig. 2, any plausible abundance of radioisotopes, even with ∼70% leaching of ^{40}K, will eventually produce enough heat to melt ice. Internal heating drives the growth of the double-diffusive convecting layer, so potassium depletion suppresses the initialization of convection throughout the entire ice/rock interior.

Double-diffusive convection involves opposing gradients of two components that have different diffusivities. With components like salt and water, both diffusivities are non-zero, and multiple convecting layers form. In Titan's ice/rock system, however, the diffusivity of the

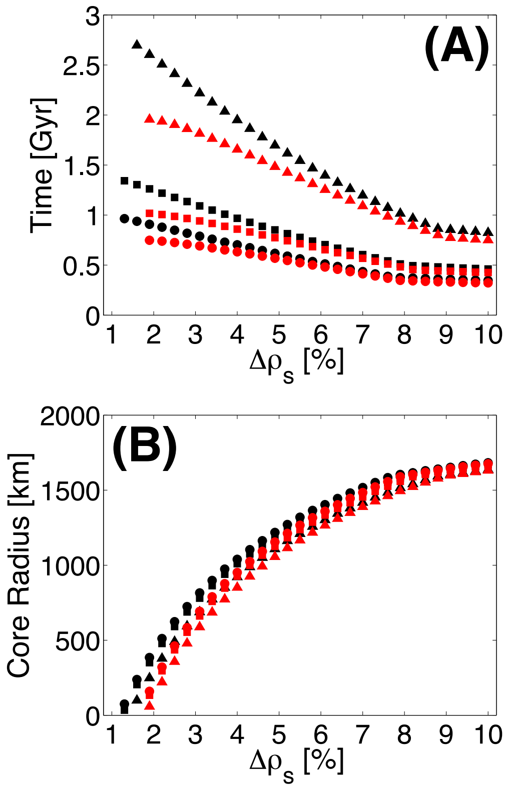

Figure 5: Details of melting during 186 simulations of Titan's thermal evolution with initial compositional gradients that produce density contrasts from $0.01\bar{\rho}$ to $0.1\bar{\rho}$ across the ice/rock interior. Panel A shows when melting occurs in the non-convecting ice/rock interior. Panel B illustrates the size of the non-convecting ice/rock core at the time when melting occurs. All simulations have $T_b = 200$ K. Black and red symbols respectively represent $T_m(0) = 125$ and 200 K. Circular, square, and triangular markers represent $f = 1.0$, 0.7, and 0.3, respectively.

rock component is effectively zero, and we only model the growth of a single layer. For small compositional gradients, the time scale for the growth of a convective instability of a new layer is much greater the time scale on which the first layer grows. With sufficiently large compositional gradients, growth of the convecting layer is slow enough that additional layers could form if melting never occurred, but melting typically occurs in ~250 to 750 Myr. In any case, heat transport through a series of convecting layers is comparatively inefficient (e.g., Turner, 1974), and the formation of many layers is unlikely to prevent complete differentiation.

5.2. Alternative internal structures

A partially differentiated Titan is a non-unique interpretation of the available gravity data (Iess et al., 2010). Because Titan's ice/rock interior is unstable to differentiation over geologic time, alternate models should be considered. One popular hypothesis is that Titan's interior is chiefly composed of hydrated silicates (e.g., Fortes et al., 2007; Castillo-Rogez and Lunine, 2010; Fortes, 2012). Three serpentine polymorphs are typically found in carbonaceous chondrites: chrysotile, lizardite, and antigorite. Antigorite is the most abundant, and its properties are usually used to track the thermochemical evolution of model assemblages (e.g., Castillo-Rogez and Lunine, 2010). After heating melts the ice component of an ice/rock mixture, redistributing rock and melt into a stable density structure with homogenized internal temperatures takes a few hundred Myr (Kirk and Stevenson, 1987; Lunine and Stevenson, 1987). The serpentinization reaction between the liberated silicates and the surrounding liquid would likely proceed to completion well before core overturn is finished (MacDonald and Fyfe, 1985).

Models assuming a core composed entirely of antigorite are missing a significant mass of iron. The formula for the magnesium end-member of antigorite is $Mg_3Si_2O_5(OH)_4$. But Fe^{2+} and Fe^{3+} often substitute into the Mg^{2+} and Al^{3+} sites, respectively, yielding a typical iron number of Fe/(Fe+Mg) $\sim$ 0.2 (Scott et al., 2002). That is, antigorite has <14 wt% Fe, significantly less than the ~18.2 wt% Fe typically found in CI chondrites (Hutchinson, 2004, p. 29). So, ~4 wt% Fe, equivalent to an Fe-rich core with a radius of a few hundred km, must accompany a mass of antigorite created from the serpentinization of silicates with chondritic composition. Some iron may be in soluble form in Titan's ocean, and the presence of a relatively small Fe-rich core may not dramatically affect Titan's moment of inertia (Castillo-Rogez and Lunine, 2010).

Figure 6 shows two end-member models for the present-day internal structure of Titan for which $C \sim 0.34$. In structure A, Titan is dominated by an hydrated silicate core with $R = 1{,}950$ km and $\bar{\rho} = 2{,}700$ kg m^{-3}. An Fe-rich core with $R = 500$ km and $\bar{\rho} = 6{,}500$ kg m^{-3}, representing ~4 wt% of the iron/rock interior is also present, although the formation of an Fe-rich core would likely dehydrate the overlying silicates. The overlying shell, composed of an ice I lid, an ocean, and high-pressure ice polymorphs, is modeled as a single layer with an average density of 1,202 kg m^{-3}. The lower ~300 km of antigorite could be replaced with dehydrated silicates in structure A without decreasing the MoI coefficient below $C \sim 0.332$

A key question is whether significant dehydration of the silicate core should be expected. The equilibrium temperature for the antigorite dehydration reaction is ~800 to 900 K for conditions appropriate to Titan (e.g., Perrillat et al., 2005), although dehydration in a water saturated environment may be kinetically hindered and not occur until temperatures reach ~1060 K (Seipold and Schilling, 2003), and the heat flux from the advection of warm water could be significant. Castillo-Rogez and Lunine (2010) found that conductive heat transport could delay significant dehydration until very recently, assuming ~30% potassium depletion and a relatively high specific heat for antigorite. Serpentine dehydration at the present may be responsible for melting clathrate hydrates in the overlying ice shell, releasing methane (Tobie et al., 2006) and radiogenic ^{40}Ar (Niemann et al., 2005) onto the surface and into the at-

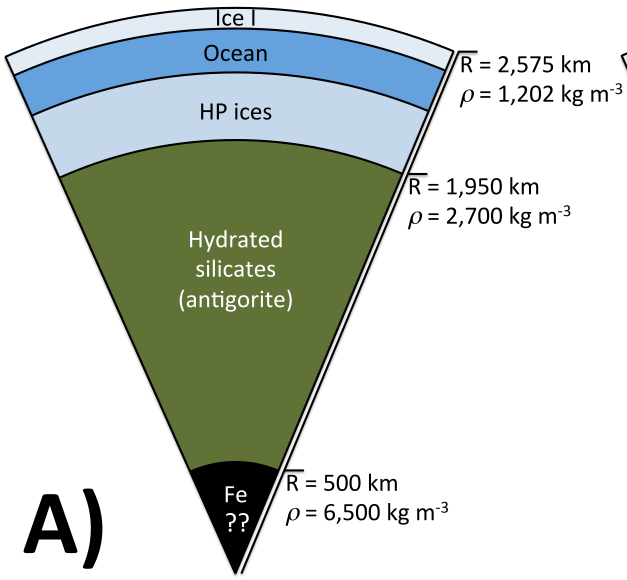

Figure 6: Two end-member internal structures for Titan that have $C \sim 0.34$. Possible material layers include an Fe-rich core, dehydrated silicates, hydrated silicates, and an ice/rock mixture. Each model includes high-pressure ices, a water ocean with dissolved gases and solids, and a layer of water ice I, all of which are modeled as a single shell with constant density. Titan's atmosphere is neither depicted nor modeled.

mosphere. We suggest that, if Titan formed partially differentiated, double-diffusive convection in the initial ice/rock mixture may have delayed core overturn for an additional $\sim$1 Gyr beyond what was assumed in Castillo-Rogez and Lunine (2010), helping the eventual core of hydrated silicates avoid dehydration.

Current data do not exclude partially differentiated models featuring a large silicate core. Structure B in Fig. 6 is an example of such a model, similar to those considered in McKinnon and Bland (2011). An ice rock mantle with R = 2,075 km, $\bar{\rho}$ = 2,200 kg m^{-3}, and $S \sim 0.63$ overlies a core of dehydrated silicates with R = 1,300 km and $\bar{\rho}$ = 3,300 kg m^{-3}. A decreased rock mass fraction and a smaller length scale for the ice/rock layer might allow efficient convection, even in the presence of a stabilizing compositional gradient. Evaluating the thermal stability of such a structure would require coupling the thermal evolution of all three layers, potentially including the effects of tidal dissipation, as has been done for Ganymede (Bland et al., 2009). More complicated variations on structure B featuring different ice/rock mixtures or a hydrated portion of the silicate core are also valid interpretations of the gravity data. Differences in the predicted tidal responses of these two models may allow discrimination between these two alternatives (Castillo-Rogez and Lunine, 2012).

5.3. Implications for other icy satellites

Gravity measurements by spacecraft suggest a spectrum of internal structures for the icy satellites of Jupiter and Saturn. The formation of an undifferentiated or a partially differentiated satellite requires a sequence of assumptions: slow accretion in a gas-starved disk, delayed to avoid catastrophic heating from the radioactive decay of short-lived isotopes, and then survival of intense impacts from the Late Heavy Bombardment (Barr and Canup, 2008, 2010; Barr et al., 2010). The Radau-Darwin approximation is primarily used to calculate the MoI of a satellite with the measured J_2 and C_{22} coefficients, but a unique solution only exists for a satellite in hydrostatic equilibrium.

Non-hydrostatic structures in the degree 2 gravity of Titan may introduce significant inaccuracies into the Radau-Darwin approximation (Gao and Stevenson, 2012). Indeed, Iess et al. (2010) reported non-hydrostatic geoid height variations as large as 19 m for Titan, possibly indicating that Titan's MoI coefficient could closer to that of Ganymede than earlier reported. The measured MoI for Callisto is likewise subject to large uncertainties because of possible non-hydrostatic effects, which are not excluded by current data (Anderson et al., 2001), but an equivalent departure from hydrostatic equilibrium would have a relatively small effect on Ganymede. The Galilean satellites are not as compositionally heterogeneous as the major Saturnian satellites (Anderson et al., 1996b,a, 1998, 2001), so the likelihood of substantial compositional gradients suppressing convection in Callisto may be lessened. In any case, the radio science instrument on the planned *JUICE* (JUpiter Icy moons Explorer) mission may allow the vastly improved measurement of the gravity fields of Ganymede and Callisto and thus the identification of gravity anomalies and significant non-hydrostatic features. With these new data, we may continue to vet the spectrum of internal differentiation states proposed for icy satellites.

6. Conclusions

Titan can survive accretion and the Late Heavy Bombardment without suffering complete differentiation if it formed slowly in a gas-starved disk, and a partially differentiated Titan is consistent with recently obtained gravity data. But radiogenic heating tends to melt ice in the undifferentiated interior over geologic time, causing irreversible sinking of the rock component. If the ice/rock interior is initially homogenous, then thermal convection may remove sufficient heat to prevent melting. Two sources of compositional gradients, however, act to suppress convection. First, Titan likely had a temperature profile immediately after accretion in which temperature decreased with depth. Second, accretion from heterogenous planetesimals would produce a stabilizing rock mass fraction gradient, where rock mass fraction and thus density increased with depth. Convection in the presence of opposing compositional and thermal gradients is “double-diffusive”, comprising a convecting layer that slowly grows from the top of the ice/rock interior. For compositional gradients larger than a few percent, this convecting layer does not grow fast enough to prevent widespread melting in the non-convecting core. A partially differentiated Titan is therefore unstable over geologic time. The general instability of ice/rock mixtures with compositional gradients may have significant consequences for other icy satellites.

7. Acknowledgments

J. G. O’Rourke thanks I. Mosqueira for helpful discussions and the NASA Planetary Geology & Geophysics Undergraduate Research Program for support.

References

Anderson, J.D., Jacobson, R.A., McElrath, T.P., Moore, W.B., Schubert, G., Thomas, P.C., 2001. Shape, mean radius, gravity field, and interior structure of Callisto. Icarus 153, 157–161, doi:10.1006/icar.2001.6664.

Anderson, J.D., Lau, E.L., Sjogren, W.L., Schubert, G., Moore, W.B., 1996a. Gravitational constraints on the internal structure of Ganymede. Nature 384, 541–543.

Anderson, J.D., Schubert, G., Jacobson, R.A., Lau, E.L., Moore, W.B., Sjogren, W.L., 1998. Europa’s differentiated internal structure: Inferences from four Galileo encounters. Science 281, 2019–2022.

Anderson, J.D., Sjogren, W.L., Schubert, G., 1996b. Galileo gravity results and the internal structure of Io. Science 272, 709–712.

Atreya, S.K., Adams, E.Y., Niemann, H.B., Demick-Montelara, J.E., Owen, T.C., Fulchignoni, M., Ferri, F., Wilson, E.H., 2006. Titan’s methane cycle. Planet. Space Sci. 54, 1177–1187, doi:10.1016/j.pss.2006.05.028.

Barr, A.C., Canup, R.M., 2008. Constraints on gas giant satellite formation from the interior states of partially differentiated satellites. Icarus 198, 163–177, doi:10.1016/j.icarus.2008.07.004.

Barr, A.C., Canup, R.M., 2010. Origin of the Ganymede-Callisto dichotomy by impacts during the late heavy bombardment. Nat. Geosci. 3, 164–167, doi:10.1038/NGEO746.

Barr, A.C., Citron, R.I., Canup, R.M., 2010. Origin of a partially differentiated Titan. Icarus 209, 858–862, doi:10.1016/j.icarus.2010.05.028.

Barr, A.C., McKinnon, W.B., 2007. Convection in ice I shells and mantles with self-consistent grain size. J. Geophys. Res. 112, E02012, doi:10.1029/2006JE002781.

Bills, B.G., Nimmo, F., 2011. Rotational dynamics and internal structure of Titan. Icarus 214, 351–355, doi:10.1016/j.icarus.2011.04.028.

Bland, M.T., Showman, A.P., Tobie, G., 2009. The orbital-thermal evolution and global expansion of Ganymede. Icarus 200, 207–221, doi:10.1016/j.icarus.2008.11.016.

Canup, R.M., 2010. Origin of Saturn’s rings and inner moons by mass removal from a lost Titan-sized satellite. Nature 468, 943–946.

Canup, R.M., Ward, W.R., 2002. Formation of the Galilean satellites: conditions of accretion. Astronom. J. 124, 3404–3423.

Castillo-Rogez, J.C., Lunine, J.I., 2010. Evolution of Titan’s rocky core constrained by Cassini observations. Geophys. Res. Lett. 37, L20205, doi:10.1029/2010GL044398.

Castillo-Rogez, J.C., Lunine, J.I., 2012. Tidal response of Titan’s interior models consistent with Cassini-derived constraints. LPSC XLIII Abstracts #1707.

Engel, S., Lunine, J.I., Norton, D.L., 1994. Silicate interactions with ammonia-water fluids on early Titan. J. Geophys. Res. 99, 3745–3752.

Fortes, A.D., 2012. Titan’s internal structure and the evolutionary consequences. Planet. Space Sci. 60, 10–17, doi:10.1016/j.pss.2011.04.010.

Fortes, A.D., Grindrod, P.M., Trickett, S.K., Vocadlo, L., 2007. Ammonium sulfate on Titan: Posible origin and role in cryovolcanism. Icarus 188, 139–153, doi:10.1016/j.icarus.2006.11.002.

Friedson, A.J., Stevenson, D.J., 1983. Viscosity of rock-ice mixtures and applications to the evolution of icy satellites. Icarus 56, 1–14.

Gao, P., Stevenson, D.J., 2012. How does nonhydrostaticity affect the determination of icy satellites’ moment of inertia? LPSC XLIII Abstracts #1701 .

Gautier, D., Hersant, F., 2005. Formation and composition of planetesimals: Trapping volatiles by clathration. Space Sci. Rev. 116, 25–52, doi:10.1007/s11214–005–1946–2.

Glein, C.R., Shock, E.L., 2010. Sodium chloride as a geophysical probe of a subsurface ocean on Enceladus. Geophys. Res. Lett. 37, L09204, doi:10.1029/2010GL042446,.

Gomes, R., Levison, H.F., Tsiganis, K., Morbidelli, A., 2005. Origin of the cataclysmic Late Heavy Bombardment period of the terrestrial planets. Nature 435, 466–469, doi:10.1038/nature03676.

Grindrod, P.M., Fortes, A.D., Nimmo, F., Feltham, D.L., Brodholt, J.P., Vocadlo, L., 2008. The long-term stability of a possible aqueous ammonium sulfate ocean inside Titan. Icarus 197, 137–151, doi:10.1016/j.icarus.2008.04.006.

Huppert, H.E., Turner, J.S., 1981. Double-diffusive convection. J. Fluid Mech. 106, 299–329.

Hutchinson, R., 2004. Meteorites. A Petrologic, Chemical and Isotopic Synthesis. Cambridge University Press.

Iess, L., Jacobson, R.A., Ducci, M., Stevenson, D.J., Lunine, J.I., Armstrong, J.W., Asmar, S.W., Racioppa, P., Rappaport, N.J., Tortora, P., 2012. The tides of Titan. Science , doi:10.1126/science.1219631.

Iess, L., Rappaport, N.J., Jacobson, R.A., Racioppa, P., Stevenson, D.J., Tortora, P., Armstrong, J.W., Asmar, S.W., 2010. Gravity field, shape, and moment of intertia of Titan. Science 327, 1367–1369 , doi:10.1126/science.1182583.

Jacobson, R.A., 2004. The orbits of the major Saturnian satellites and the gravity field of Saturn from spacecraft and Earth-based observations. Astrophys. J. 128, 492–501, doi:10.1086/421738.

Jaumann, R., Kirk, R.L., Lorenz, R.D., Lopes, R.M.C., Stofan, E., Turtle, E.P., Keller, H.U., Wood, C., Sotin, C., Soderblom, L.A., Tomasko, M.G., 2009. Geology and surface processses on Titan, in: Brown, R.H., Lebreton, J.P., Waite, J.H. (Eds.), Titan from Cassini-Huygens. Springer. chapter 5.

Kirk, R.L., Stevenson, D.J., 1987. Thermal evolution of a differentiated Ganymede and implications for surface features. Icarus

69, 91–134.
Lissauer, J.J., Stevenson, D.J., 2007. Formation of giant planets, in: Reipurth, B., Jewitt, D., Keil, K. (Eds.), Protostars and Planets V. University of Arizona Press, Tucson, pp. 591–606.
Loveday, J.S., Nelmes, R.J., Bull, C.L., Maynard-Casely, H.E., Guthrie, M., 2009. Observation of ammonia dihydrate in the AMH-VI structure at room temperature - possible implications for the outer solar system. High Pressure Res. 29, 396–404, doi:10.1080/08957950903162057.
Lunine, J., Choukroun, M., Stevenson, D.J., Tobie, G., 2009. The origin and evolution of Titan, in: Brown, R.H., Lebreton, J.P., Waite, J.H. (Eds.), Titan from Cassini-Huygens. Springer. chapter 3.
Lunine, J.I., Stevenson, D.J., 1987. Clathrate and ammonia hydrates at high pressure: Application to the origin of methane on Titan. Icarus 70, 61–77.
MacDonald, A.H., Fyfe, W.S., 1985. Rate of serpentinization in seafloor envrionments. Tectonophysics 116, 123–135, doi:10.1016/0040–1951(85)90225–2.
McKinnon, W.B., 1997. Mystery of Callisto: Is it undifferentiated? Icarus 130, 540–543, doi:10.1006/icar.1997.5826.
McKinnon, W.B., Bland, M.T., 2011. Core evolution in icy satellites and Kuiper belt objects. LPSC XLII Abstracts #2768.
Mitri, G., Pappalardo, R.T., Stevenson, D.J., 2010. Evolution and interior structrure of Titan. LPSC XLI Abstracts #2229 .
Mitri, G., Showman, A.P., 2008. Thermal convection in ice-I shells of Titan and Enceladus. Icarus 193, 387–396, doi:10.1016/j.icarus.2007.07.016.
Mosqueira, I., Estrada, P.R., 2003a. Formation of the regular satellites of giant planets in an extended gaseous nebula I: subnebula model and accretion of satellites. Icarus 163, 198–231, doi:10.1016/S0019–1035(03)00076–9.
Mosqueira, I., Estrada, P.R., 2003b. Formation of the regular satellites of giant planets in an extended gaseous nebula II: satellite migration and survival. Icarus 163, 232–255, doi:10.1016/S0019–1035(03)00077–0.
Mosqueira, I., Estrada, P.R., Charnoz, S., 2010. Deciphering the origin of the regular satellites of gaseous giants — Iapetus: The Rosetta ice-moon. Icarus 207, 448–460, doi:10.1016/j.icarus.2009.10.018.
Mueller, S., McKinnon, W.B., 1988. Three-layered models of Ganymede and Callisto: Compositions, structures, and aspects of evolution. Icarus 76, 437–464.
Nagel, K., Breuer, D., Spohn, T., 2004. A model for the interior structure, evolution, and differentiation of Callisto. Icarus 169, 402–412, doi:10.1016/j.icarus.2003.12.019.
Niemann, H.B., Atreya, S.K., Bauer, S.J., Carignan, G.R., Demick, J.E., Frost, R.L., Gautier, D., Haberman, J.A., Harpold, D.N., Hunten, D.M., Israel, G., Lunine, J.I., Kasprzak, W.T., Owen, T.C., Paulkovich, M., Raulin, F., Raaen, E., Way, S.H., 2005. The abundances of constituents of Titan's atmospehre from the GCMS instrument on the Huygens probe. Nature 438, 779–784, doi:10.1038/nature04122.
Nimmo, F., Bills, B.G., 2010. Shell thickness variations and the long-wavelength topography of Titan. Icarus 208, 896–904, doi:10.1016/j.icarus.2010.02.020.
Noguchi, T., Niino, H., 2010. Multi-layered diffusive convection. Part 1. Spontaneous layer formation. J. Fluid Mech. 651, 443–464, doi:10.1017/S0022112009994150.
Perrillat, J.P., Daniel, I., Koga, K.T., Reynard, B., Cardon, H., Crichton, W.A., 2005. Kinetics of antigorite dehydration: A real-time X-ray diffraction study. Earth Planet. Sci. Lett. 236, 899–913, doi:10.1016/j.epsl.2005.06.006.
Petrenko, V.F., Whitworth, R.W., 1999. Physics of Ice. Oxford University Press.
Ransford, G.A., Finnerty, A.A., Collerson, K.D., 1981. Europa's petrological thermal history. Nature 289, 21–24, doi:10.1038/289021a0.
Raulin, F., McKay, C., Lunine, J., Owen, T.C., 2009. Titan's astrobiology, in: Brown, R.H., Lebreton, J.P., Waite, J.H. (Eds.), Titan from Cassini-Huygens. Springer. chapter 9.
Rempel, A.W., Wettlaufer, J.S., Worster, M.G., 2001. Interfacial premelting and the thermomolecular force: Thermodynamic buoyancy. Phys. Rev. Lett. 87, 088501, doi:10.1103/PhysRevLett.87.088501.
Schmitt, R.W., 1983. The characteristics of salt fingers in a variety of fluid systems, including stellar interiors, liquid metals, oceans, and magmas. Phys. Fluids 26, 2373–2377.
Schmitt, R.W., 1994. Double diffusion in oceanography. Annu. Rev. Fluid Mech. 26, 255–285.
Scott, H.P., Williams, Q., Ryerson, F.J., 2002. Experimental constraints on the chemical evolution of large icy satellites. Earth Planet. Sci. Lett. 203, 399–412.
Seipold, U., Schilling, F.R., 2003. Heat transport in serpentinites. Tectonophysics 370, 147–162, doi:10.1016/S0040–1951(03)00183–5.
Simoes, F., Pfaff, R., Hamelin, M., Klenzing, J., Freudenreich, H., Beghin, C., Berthelier, J.J., Bromund, K., Grard, R., Lebreton, J.P., Martin, S., Rowland, D., Sentman, D., Takahashi, Y., Yair, Y., 2012. Using Schumann resonance measurements for constraining the water abundance on the giant planets—Implications for the Solar System's formation. Astrophys. J. 750, 85, doi:10.1088/0004–637X/750/1/85.
Sohl, F., Hussmann, H., Schwentker, B., Spohn, T., Lorenz, R.D., 2003. Interior structure models and tidal Love numbers of Titan. J. Geophys. Res. 108, 5130, doi:10.1029/2003JE002044.
Sohl, F., Spohn, T., Breuer, D., Nagel, K., 2002. Implications from Galileo observations on the interior structure and chemistry of the Galilean satellites. Icarus 157, 104–119, doi:10.1006/icar.2002.6828.
Sotin, C., Mitri, G., Rappaport, N.J., Schubert, G., Stevenson, D.J., 2009. Titan's interior structure, in: Brown, R.H., Lebreton, J.P., Waite, J.H. (Eds.), Titan from Cassini-Huygens. Springer. chapter 4.
Spiegel, E.A., 1972. Convection in stars II. Special effects. Ann. Rev. Astron. Astophys. 10, 261–3044.
Stern, M.E., 1960. The "salt-fountain" and thermohaline convection. Tellus 12, 172–175.
Tobie, G., Gautier, D., Hersant, F., 2012. Titan's bulk composition constrained by *Cassini-Huygens*: Implication for internal outgassing. Astrophys. J. 752, 125, doi:10.1088/0004–637X/752/2/125.
Tobie, G., Lunine, J.I., Sotin, C., 2006. Episodic outgassing as the origin of atmospheric methane on Titan. Nature 440, 61–64 , doi:10.1038/nature04497.
Tobie, G., Mocquet, A., Sotin, C., 2005. Tidal dissipation within large icy satellites: Applications to Europa and Titan. Icarus 177, 534–549, doi:10.1016/j.icarus.2005.04.006.
Travis, B.J., Schubert, G., 2005. Hydrothermal convection in carbonaceous chondrite parent bodies. Earth Planet. Sci. Lett. 240, 234–250, doi:10.1016/j.epsl.2005.09.008.
Tsiganis, K., Gomes, R., Morbidelli, A., Levison, H.F., 2005. Origin of the orbital architecture of the giant planets of the Solar System. Nature 435, 459–461, doi:10.1038/nature03539.
Turner, J.S., 1973. Buoyancy Effects in Fluids. Cambridge University Press, New York: New York.
Turner, J.S., 1974. Double-diffusive phenomena. Ann. Rev. Fluid Mech. 6, 37–54.
Turner, J.S., 1985. Multicomponent convection. Ann. Rev. Fluid Mech. 17, 11–44.
Veronis, G., 1968. Effect of a stabilizing gradient of solute on thermal convection. J. Fluid Mech. 34, 315–336.
Worster, M.G., 2004. Time-dependent fluxes across double-diffusive interfaces. J. Fluid Mech. 505, 287–307, doi:10.1017/S0022112004008523.